STRUCTURAL AND OPTICAL CHARACTERIZATION OF Ce-DOPED $BaTiO_3$ THIN FILMS PREPARED BY THE SOL-GEL METHOD

Elena Mirabela SOARE[1], Roxana TRUȘCĂ[2], Mihai ANASTASESCU[3], Adelina IANCULESCU[4], Măriuca GARTNER[4,*], Cătălina Andreea STANCIU[2,5 *]

In this paper, we report on the synthesis, structural and microstructural characterization, and optical properties of cerium-doped barium titanate ($Ba_{0.95}Ce_{0.05}Ti_{0.9875}O_3$) thin films. Si-Pt/$Ba_{0.95}Ce_{0.05}Ti_{0.9875}O_3$ thin films were prepared by spin coating from a sol precursor of $Ba_{0.95}Ce_{0.05}Ti_{0.9875}O_3$. We used an original acetate route of the sol-gel technique to synthesize a clear, homogeneous, and stable sol precursor. The $Ba_{0.95}Ce_{0.05}Ti_{0.9875}O_3$ thin film of ~140 nm thickness, crystallized by annealing at 700 °C for 1 hour in the air. The as-prepared $Ba_{0.95}Ce_{0.05}Ti_{0.9875}O_3$ thin films show higher crystallinity, uniform microstructure, and good optical properties for many electro-optic applications.

Keywords: Thin-film, Ce^{3+} doped $BaTiO_3$, Sol-gel, Optical properties, Structure and microstructure

1. Introduction

The properties of ferroelectric materials depend on a variety of factors, such as composition, microstructure, and surface conditions (mechanical and electrical) [1]. Dielectric, ferroelectric, pyroelectric, and piezoelectric properties were obtained for doped $BaTiO_3$. For a specific composition, the properties are

[1] PhD student, Department of Science and Engineering of Oxide Materials and Nanomaterials, Faculty of Chemical Engineering and Biotechnology, National University of Science and Technology POLITEHNICA of Bucharest, Romania, e-mail: msoare@icf.ro; e.msoare96@gmail.com

[2] PhD Eng., Scientific Researcher, Department of Science and Engineering of Oxide Materials and Nanomaterials, Faculty of Chemical Engineering and Biotechnology, National University of Science and Technology POLITEHNICA of Bucharest, Romania

[3] PhD. Eng., Scientific Researcher, Department of Surface Chemistry and Catalysis, Institute of Physical Chemistry "Ilie Murgulescu", Romanian Academy, Bucharest, Romania.

[4] PhD. Eng., Scientific Researcher, Department of Surface Chemistry and Catalysis, Institute of Physical Chemistry "Ilie Murgulescu", Romanian Academy, Romania, e-mail: mfgartner@yahoo.com

[5] PhD. Eng., Scientific Researcher, Department of Solid-State Quantum Electronics, National Institute for Laser, Plasma and Radiation Physics, Măgurele Platform, Bucharest - Ilfov County, Romania, e-mail: catalina.a.stanciu@gmail.com

different if the system is a monocrystal, powder, polycrystalline ceramic, or a thin film deposited on a substrate.

Thin film materials have attracted significant attention in integrated optics, presenting a reasonable challenge in creating low-loss and low-cost thin films for optical application devices. The excessive interest in thin film materials arises from the need for high dielectric constant materials used in bypass capacitors for VLSI technology and materials for memory access. Especially from technological applications and academic perspectives, these types of materials attract considerable interest due to their diverse range of physical properties, like hysteresis behavior, rapid switching speed, and spontaneous polarization below the Curie temperature [2].

Thin film devices exhibit physical properties that are better than those made in bulk. Major differences in the refractive indices of the film and substrate create waveguides with high confinement, making them especially favorable for rapid electro-optic switching at low voltages. Furthermore, thin film geometry simplifies the process of achieving effective index changes along the length of the waveguide. It can also function as photonic band gap geometries or Bragg reflectors [3].

Among others, barium titanate ($BaTiO_3$, BTO) is the most widely used ferroelectric material with applications in many fields, such as optics and electronics [4]. It presents the ABO_3 perovskite structure, which is found in different crystallographic variants influenced by temperature. When heated, donor-doped barium titanate exhibits a tetragonal to cubic phase transition near the Curie temperature. The tetragonal phase displays ferroelectric properties, while the cubic phase exhibits paraelectric behavior [5]. During the transition from tetragonal to cubic, the electrical resistance of the material increases by several orders of magnitude. The magnitude and steepness of this resistance increase are influenced by the sintering schedule, particularly the cooling rate, and the concentrations of dopants used in the material [6].

$BaTiO_3$ serves as a promising thin film integrated optic host due to its significant electro-optic features. Many studies were concentrated on single-crystal and ceramic $BaTiO_3$; nevertheless, thin films are increasingly utilized in various applications. Many techniques are typically used to fabricate these thin films, including hydrothermal methods, electrochemical reduction, molecular beam epitaxy, sputtering, metalorganic deposition, chemical vapor deposition, and the sol-gel process [7], [8]. In the sol–gel technique, the precursor sol is prepared in the first step, and then the sol is deposited on the substrate using techniques like spin or dip coating. Besides coating, a thin film crystallization step requires a subsequent calcination process, which is generally needed. The increase of heating rates in the calcination step resulted in nanostructured films in a shorter time, and may improve the densification rate.

The piezoelectric generation of perovskite $BaTiO_3$ thin films on a flexible substrate has been applied to convert mechanical energy to electrical energy [9]. Therefore, barium titanate remains the most important ceramic [8] dielectric applied in power electronics, biomedical applications, and optical applications [10], [11]. $BaTiO_3$ is one of the efficient candidates for photocatalysis due to its ferroelectric property [12]. Also, $BaTiO_3$ is a technologically relevant material in the perovskite oxide class with above-room-temperature ferroelectricity and a very large electro-optical coefficient, making it highly suitable for emerging electronic and photonic devices. To enhance the dielectric, ferroelectric, optical, and tunability properties of thin films, it has been proposed to create multi-layered films using multiple identical deposition–annealing cycles and doping the $BaTiO_3$ lattice [5].

Doping in $BaTiO_3$-type ceramics plays an important role in the improvement of their performance [13]. The effect of Ce doping in $BaTiO_3$ ceramic materials has shown promising dielectric properties such as a relatively high permittivity, a decrease in Curie point temperature, and high endurance. Cerium can exist in two oxidation states, 4+ and 3+. Hwang and Han suggested that when cerium oxide (CeO_2) was added to $BaTiO_3$, Ce^{3+} was incorporated into the Ba^{2+} sites instead of the Ti^{4+} sites [14]. When $BaTiO_3$ and CeO_2 are sintered in the presence of air with an additional amount of TiO_2, Ce is incorporated as a donor at the Ba-ion sites of $BaTiO_3$ [15]. On the other hand, when sintering is operated in $BaTiO_3$ and CeO_2 with an excess amount of BaO, Ce is incorporated at the Ti sites [15] . In the perovskite structure of $BaTiO_3$, with the general formula ABO_3, the '*A*' sites are occupied by larger cations of Ba^{2+}, and the '*B*' sites are occupied by smaller cations of Ti^{4+}. When Ce^{3+} ions are incorporated into the *A* sites (*i.e.*, substituting for Ba^{2+}), they introduce extra electrons into the system and thus act as donor dopants [16], while when Ce^{4+} ions occupy the Ti^{4+} (*B*) sites, it maintains charge neutrality relative to Ti^{4+} and forms a homovalent solid solution [17].

Another assumption presents the formation of an equal number of barium and titanium vacancies for the compensation of donor excess charge. The achievable reaction to the incorporation of cation vacancies in the equimolar addition of CeO_2:TiO_2 into the barium titanate lattice, where the defect notation used is Kröger and Vink, is presented below[14]:

$$6CeO_2 + 6TiO_2 \rightarrow 6Ce_{Ba}^{\bullet} + 6Ti_{Ti}^{x} + V_{Ba}^{"} + V_{Ti}^{''''} + 21O_O^x + {}^3/_2\, O_2(g) \quad (1)$$

In this case, a single-phase perovskite with nominal formula $Ba_{1-7x/6}Ce_xTi_{1-x/6}O_3$ would be obtained. As described by Eq. (1), the donor impurities are compensated by barium and titanium vacancies. The cation vacancy ($V_{Ti}^{''''}$) is reflected as an unlikely defect due to its elevated effective charge [18].

The Ba/Ti ratio and oxygen partial pressure depend on the oxidation state of cerium, its site occupancy, and its solubility in the host $BaTiO_3$ lattice. Various methods have been used to fabricate Ce-$BaTiO_3$ thin films, such as RF-magnetron sputtering[19], [20], pulsed laser deposition (PLD) [21], electron beam evaporation method [22], aerosol deposition method (ADM) [23], rapid thermal two-stage metal-organic chemical vapor deposition [24], direct vapor deposition [25], and sol-gel method [26], etc. The fabrication employed the sol-gel method because of its advantages, such as easy operation, stoichiometry control, and low-cost equipment [27].

This work aims to prepare by sol-gel method coupled with the spin-coating deposition technique, a Si-Pt/$Ba_{0.95}Ce_{0.05}Ti_{0.9875}O_3$ thin film without cracks, with good adhesion to the substrate, well crystallized, with a smooth surface, with stoichiometric chemical composition, and with good functional properties. As a result, their structural, microstructural, and optical properties are investigated and discussed here.

2. Experimental

2.1. Materials and preparation of precursor sol and BCT thin films

Barium acetate ($Ba(CH_3COO)_2$, 99%), titanium (IV) isopropoxide ($Ti(OCH(CH_3)_2)_4$, 97%) in 2-propanol, cerium acetate ($Ce(CH_3CO_2)_3$, 99.9%), acetic acid (CH_3-COOH, 99.5%), 2-methoxyethanol ($C_3H_8O_2$, 99%) and acetylacetone ($CH_3COCH_2COCH_3$, 97%) were used as starting materials to prepare $Ba_{0.95}Ce_{0.05}Ti_{0.9875}O_3$ sol precursor for BTCO thin films. All reagents are provided by Sigma-Aldrich. Pt/TiO_2/SiO_2/Si (abbreviated as Si-Pt) was used as a substrate for BTCO thin film, Si-Pt/$Ba_{0.95}Ce_{0.05}Ti_{0.9875}O_3$.

BCT films with the nominal formula $Ba_{0.95}Ce_{0.05}Ti_{0.9875}O_3$ have been prepared by the acetate sol-gel method described in Fig.1. Two different solutions were prepared by dissolving appropriate amounts of barium acetate and cerium acetate in acetic acid at 80 °C, under continuous stirring. These solutions were stabilized by using 2-methoxyethanol and acetylacetone in a 2:1 volume ratio. Another solution was prepared by mixing titanium isopropoxide in 2-propanol. The barium acetate solution was added to the titanium isopropoxide solution under continuous stirring. Then, the cerium acetate solution was added to the barium and titanium mixture solution. In a subsequent step, acetylacetone was added to the as-obtained solution. The resulting clear, yellowish sol was then heated on a hot plate under magnetic stirring at 80 °C for 3 h for better homogenization. The as-obtained sol precursor was used for the deposition of $Ba_{0.95}Ce_{0.05}Ti_{0.9875}O_3$ thin film. The $Ba_{0.95}Ce_{0.05}Ti_{0.9875}O_3$ thin film was deposited by spin-coating on a Si-Pt substrate. The Si-Pt substrate also contains two layers, SiO_2 and TiO_2, so the structure of the Si-Pt substrate is Si/SiO_2/TiO_2/Pt. The SiO_2 layer is difficult to remove from the silicon layer because it is very easily formed

by the oxidation of silicon with atmospheric humidity. For some applications, the SiO_2 layer on Si is useful, and in this case, the desired thickness of the SiO_2 layer can be achieved by oxidizing the surface of the Si layer with water vapor at 700 °C. TiO_2 is widely used for adhesion of the Pt bottom electrode because the Pt thin films often have poor adhesion to the SiO_2/Si substrate. The Si-Pt substrate used in this work has the following thicknesses: 200 µm Si/450 nm SiO_2/15 nm TiO_2/100nm Pt, as sold by the manufacturer. The film of $Ba_{0.95}Ce_{0.05}Ti_{0.9875}O_3$ was deposited from the precursor sol by the spin-coating technique at 3000 rpm for 20 seconds on the Si-Pt substrate. Then, the gel film was dried at 200 °C for 2 min to evaporate the solvent. Then, the dried layer was pyrolyzed at 400 °C for 4 min, in air, for organic components removal. The film was prepared by repeating (10 times) the deposition and pyrolysis cycle. The final thermal treatment (for the 10 layers deposited) was performed at 700°C for 1 hour, with a heating rate of 5°C/min (optimal thermal conditions for our thin films). The flowchart of the preparation of BCT films is presented in Fig. 1, and the substrate structure $Si/SiO_2/TiO_2/Pt$ is shown in Fig. 2.

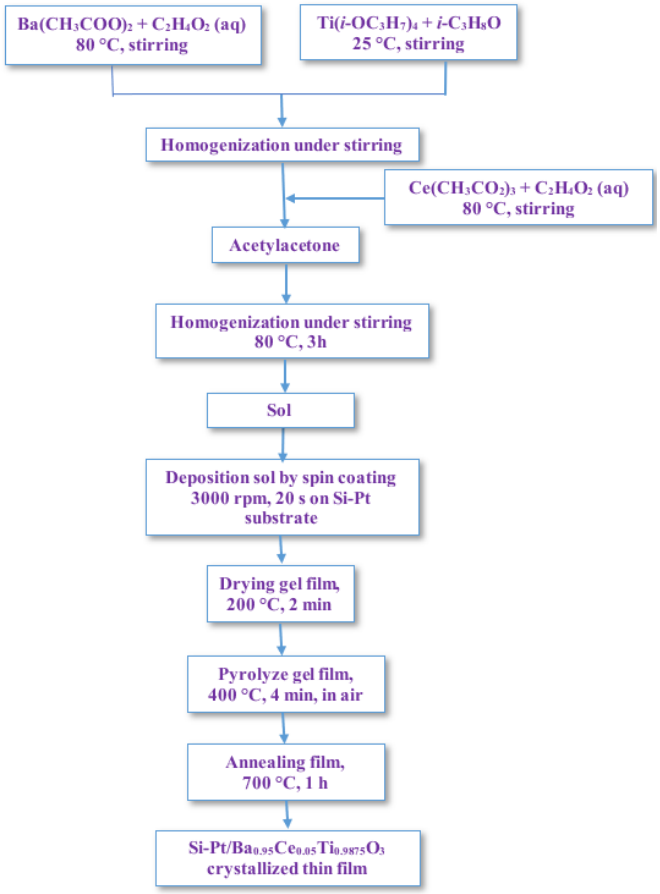

Fig. 1. The flowchart of BCT thin films

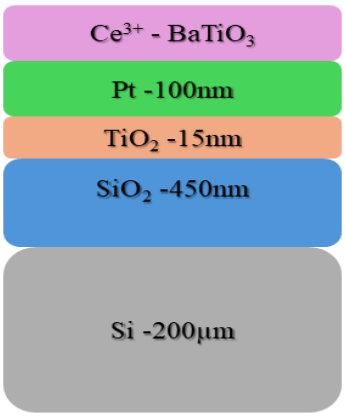

Fig.2. Multi-layer support structure for $Ba_{0.95}Ce_{0.05}Ti_{0.9875}O_3$

2.2. Characterization of BCT thin films

The crystal structure of the thin films was analyzed using X-ray diffraction with a Shimadzu XRD 600 diffractometer, employing Ni-filtered CuKα radiation. The scan step increments were set at 0.02°, with a counting time of 1 s/step, for a 2θ range of 20° to 60°. The surface and cross–section morphology of the thin films and their thickness were investigated through Scanning Electron Microscopy (SEM) in backscattering mode (BSE) with a QUANTA INSPECT.F microscope equipped with a field emission electron source gun. For the optical characteristics of the films regarding optical constants (refraction index *n* and extinction coefficient *k*), a Spectroscopic Ellipsometry (SE) was utilized. The measurements were conducted in ambient atmosphere over a wavelength range of 200–1700 nm, with increments of 10 nm, at an incidence angle of 70° using VASE–Woollam equipment equipped with a rotating analyzer and AutoRetarder. Detection was achieved through a photodiode that includes an integrated preamplifier, utilizing digital lock-in hardware. The SE spectra were analyzed using the Bruggemann Effective Medium Approximation (B–EMA) [28], [29].

3. Results and discussion

3.1. Phase and Structural Characterization

Fig. 3 shows the XRD pattern of $Ba_{0.95}Ce_{0.05}Ti_{0.9875}O_3$ thin film deposited on Si-Pt substrate and calcined at 700 °C for 1 hour, in air.

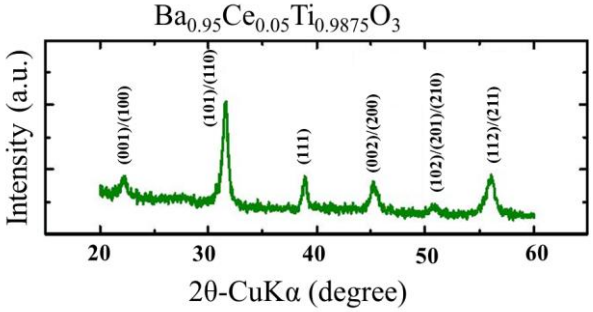

Fig. 3. X-ray diffractogram of the films of $Ba_{0.95}Ce_{0.05}Ti_{0.9875}O_3$ calcined at 700 °C, 1 h in air.

Diffraction peaks of $Ba_{0.95}Ce_{0.05}Ti_{0.9875}O_3$ calcined at 700 °C for 1 hour, in air, could be indexed by a single-phase perovskite structure, and no secondary phase appeared. The presence of sharp and well-defined peaks indicates a crystalline thin film. All the peaks are indexed (identified using JCPDS card code: 96-151-3253) [16] for cubic $BaTiO_3$ phase formation, which belongs to space group *Pm-3m*.

The slight shift in peak positions compared to pure $BaTiO_3$ suggests successful Ce doping. Ce^{3+} substitution for Ba^{2+} or Ti^{4+} can induce lattice distortion, slightly shifting peak angles. According to Fig. 3, the thin film of $Ba_{0.95}Ce_{0.05}Ti_{0.9875}O_3$ shows a polycrystalline structure, without any preferred orientation for crystallization. The film is well crystallized and exhibits a pseudocubic structure, with lattice parameters a = c = 4.0281(14) Å. The similarity between the a and c parameters in a slightly distorted perovskite is typical for $BaTiO_3$ systems. Doping with Ce^{3+} often causes distortions of the unit cell. The volume of the unit cell is V = 65.36 $Å^3$, and the average crystallite size = 293(36) Å. This is a bit smaller than the volume of the undoped $BaTiO_3$ (typically ~65.8–66 $Å^3$), indicating a slight lattice contraction, which suggests that Ce^{4+} (ionic radius ~0.87 Å) substitutes for the larger Ba^{2+} (1.35 Å). Such contraction is expected and supports that Ce is well-incorporated into the lattice, rather than forming separate phases.

All the notable peaks in the cerium-doped barium titanate film present a structure with orientation along (100), (111), (200), and (211) planes [30]. The lack of peaks corresponding to secondary phases demonstrates the incorporation of Ce^{3+} ions in the $BaTiO_3$ lattice. These characteristics are ideal for applications requiring good ferroelectric, dielectric, or sensor behavior, particularly if a high degree of structural integrity and phase purity is needed.

The uniformity and quality of the annealed $Ba_{0.95}Ce_{0.05}Ti_{0.9875}O_3$ thin film at 700 °C for 1 hour can be observed in the SEM images (Fig. 4).

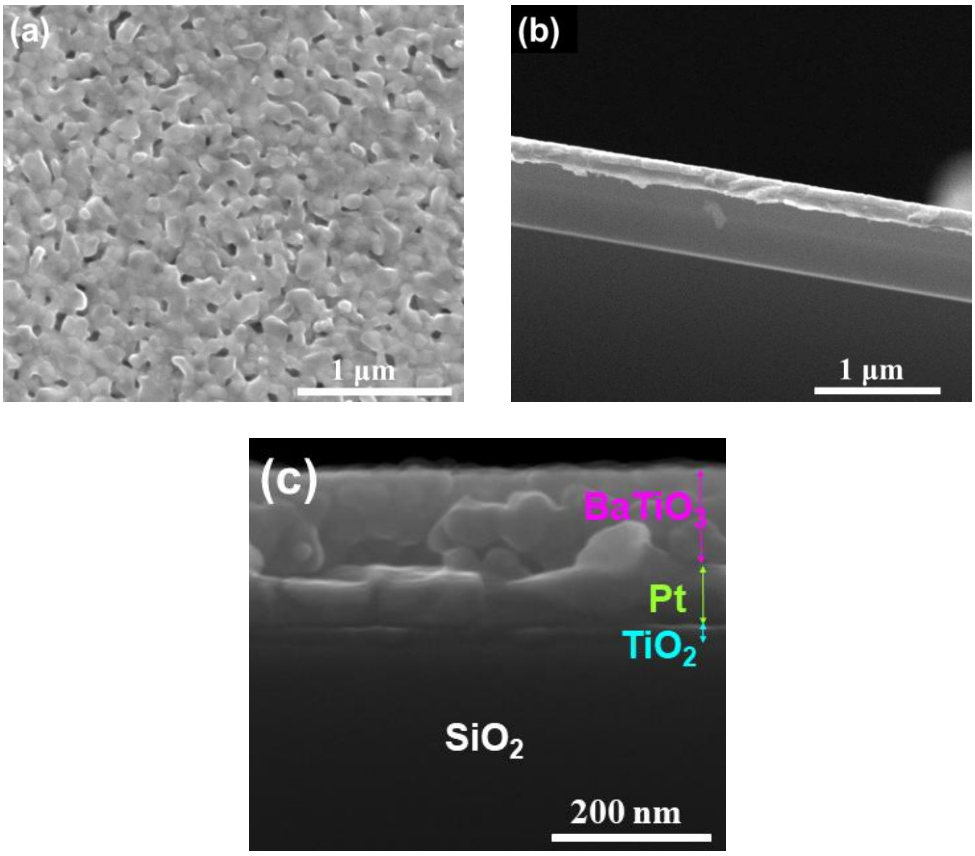

Fig. 4. (a) SEM images of the surface of $Ba_{0.95}Ce_{0.05}Ti_{0.9875}O_3$ thin film deposited on Si-Pt substrate and calcined at 700 °C for 1 hour, in air, (b) SEM images in cross-section for the films of $Ba_{0.95}Ce_{0.05}Ti_{0.9875}O_3$ and (c) detailed image for cross-section

The SEM overview image in cross-section highlights the production of a continuous film with uniform thickness, free from defects and delamination, indicating that the deposited film had good adhesion to the substrate, good film quality, and homogeneous growth (Fig. 4 (b)). A detailed SEM image shows that the cross-sectional microstructure is homogeneous and dense, indicating a growing polycrystalline mechanism of the "layer-by-layer" type, specific for sol-gel deposits, as presented in Fig. 4 (c). The estimated thickness based on the SEM image in the section of the BCT film is approximately 140 nm. The surface is also uniform, free of cracks, with a dense microstructure, finely granulated, with a monomodal grain size distribution, consisting of homogeneous crystalline grains, with an average size of approximately 35 nm (Fig. 4 (a)). The grain size looks to be in the nanometer range, which is typical for sol-gel or sputtered thin films.

The films have homogeneous surface microstructure and thickness. The image in Fig. 4 shows the surface morphology of $Ba_{0.95}Ce_{0.05}Ti_{0.9875}O_3$ thin film,

indicating a microstructure of grains with elongated shapes and variable sizes. Some intergranular pores can be observed on the film surface due to solvent evaporation, which is characteristic of the films prepared by the sol-gel method. The average thickness of the films deduced from the SEM cross-section images is ~140 nm (Fig. 4(b) and Fig. 4(c)). This kind of morphology is beneficial for applications in electronics or sensors, as it suggests good mechanical integrity and possibly low leakage currents.

4. Optical properties

$BaTiO_3$ has a bandgap energy of approximately 3.2 eV and does not support low-energy excitons. As a result, it serves as an optical dielectric with a moderately refractive index of around 2.5 and minimal optical losses at visible and near-infrared wavelengths [31]. This material is well-suited for use in photonic waveguides due to its low optical losses, as well as in resonant nanostructures, such as photonic metasurfaces, photonic crystals, and other nanostructures, because of its significant refractive index contrast compared to substrates like quartz. In its single-crystal form, the tetragonal phase exhibits birefringent optical properties.

The anisotropy seen under an optical microscope led to the use of the New Amorphous Dispersion Model, derived from the Forouhi and Bloomer (F-B) amorphous model, to compute the thin film's refractive index and extinction coefficient [31].

The refractive index is connected to the electronic polarizability of a material and the concentration of polarizable constituents within the system. The classical law of refraction can be deduced from the Lorenz formula [32]:

$$\frac{n^2-1}{n^2+2}=\frac{4\pi}{3}N\alpha \tag{2}$$

Where n represents the refractive index, N is the number density of polarizable units, and α is the electronic polarizability.

Following Eq. (2), the increase of material density (meaning the increase in N) tends to produce a larger refractive index as long as polarizability does not increase significantly [32] - [34].

The Cauchy model is applied for the Ce^{3+} doped BTO thin film and is valid in the transparent region of the spectrum for this film. The value of mean square error (MSE) was 9.77 and indicated a good fit. The following formula expresses the refractive index:

$$n(\lambda)=A+\frac{B}{\lambda^2}+\frac{C}{\lambda^4} \tag{3}$$

Where: λ= wavelength (nm); A, B, and C indicate the empirical fitting constants.

Based on the Cauchy model, the Ce-doped BTO thin film is quite transparent in the 300-900 nm spectrum. Thicknesses and stack configuration are vital for precise modeling, and a layered stack was crucial for the decent fit of the model (MSE = 9.77). However, increasing k with higher wavelengths indicates the onset of absorption or possible measurement effects. These issues might be addressed by another model (Tauc-Lorentz model) for more accurate predictions beyond this range.

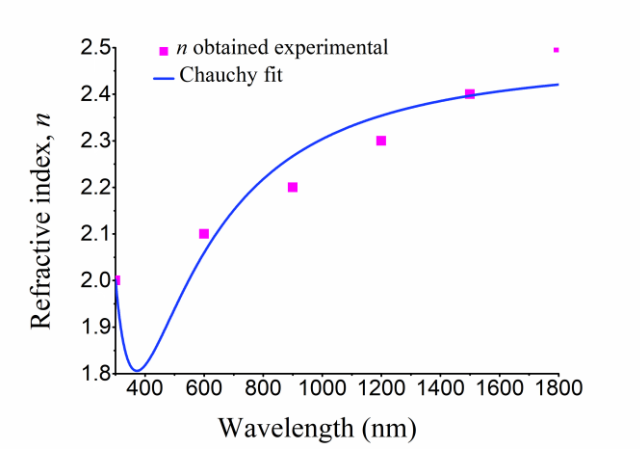

Fig 5. The Chauchy model fit coefficients for $Ba_{0.95}Ce_{0.05}Ti_{0.9875}O_3$ thin film

As we can observe, the index increases with wavelength, which is unusual for dielectric materials and might hint at the underlying material effects or limitations of applying the Cauchy model in this region.

Table 1

n and k coefficients for the $Ba_{0.95}Ce_{0.05}Ti_{0.9875}O_3$ thin film

Wavelength (nm)	Refractive index, *n*	Extinction Coefficient, *k*
300	2.00	0.00
600	2.10	0.03
900	2.20	0.06
1200	2.30	0.09
1500	2.40	0.12
1800	2.50	0.15

Another model that we used is the Tauc-Lorentz model. The optical constants (n, k), obtained from the fitting (between experimental and simulated data), are shown in Fig. 6. It is known that the optical constants of thin films vary with the degree of crystallization, uniformity, and size of crystallites, number of structural defects, and film surface roughness. A common characteristic of thin

oxidative films produced via the derived sol-gel method is a high percentage of defects in the initial deposited layer.

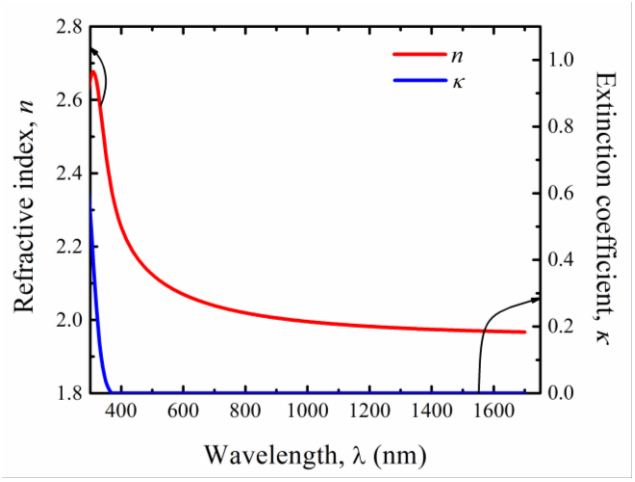

Fig. 6. The variation of optical properties with wavelength, λ, for $Ba_{0.95}Ce_{0.05}Ti_{0.9875}O_3$ thin films: refraction index *n* and extinction coefficient *k*

As it can be seen in Fig. 6, the refraction index *n* decreases up to *n*=1.9 as the wavelength increases up to *λ*=1700 nm, while the extinction coefficient *k* drops sharply to values close to zero at wavelengths of ~ 400 nm, for $Ba_{0.95}Ce_{0.05}Ti_{0.9875}O_3$ thin films. This can be attributed to the rising frequency of thermal treatments along with the addition of a new layer, combined with the observation that the new layer develops on a more "orderly" previous layer. Also, it can be seen that Ce doping leads to an advance in the refractive index of the film. However, the value becomes constant above the wavelength of 1100 nm. The alteration shows that a structural modification occurred due to doping during the synthesis process. A high refractive index causes the $Ba_{0.95}Ce_{0.05}Ti_{0.9875}O_3$ to be viable for anti-reflection coating [27].

5. Conclusions

In summary, $Ba_{0.95}Ce_{0.05}Ti_{0.9875}O_3$ thin films of ~ 140 nm thickness were successfully deposited on a Si-Pt substrate using the sol-gel and spin coating deposition method. These thin films show a single-phase perovskite structure of the cubic $BaTiO_3$ phase, as determined from XRD investigations. By adjusting the manufacturing conditions until optimization (precursor soil concentration, spin coating deposition parameters, sequential heat treatment conditions), we have demonstrated in this work that the high morpho-structural quality Ce-doped $BaTiO_3$ thin films can be fabricated using our protocol. The optical constants (*n*,

k) values of $Ba_{0.95}Ce_{0.05}Ti_{0.9875}O_3$ thin films indicated that the thin films, as-prepared, show good optical properties. By the results of analysis and measurements, this paper highlights the possibility of fabricating cerium-doped $BaTiO_3$ thin films by sol-gel and spin coating deposition techniques, with remarkable optical properties for applications as optoelectronic devices.

REFERENCES

[1] I. Adelina, "On size effect related to the ferroelectricity preservation in $BaTiO_3$ - based micro- and nanostructured system," Rom. J. Mater., **vol. 37**, no. 3, p. 167, 2007.

[2] A. I. Kingon, S. K. Streiffer, C. Basceri, and S. R. Summerfelt, "High-Permittivity Perovskite Thin Films for Dynamic Random-Access Memories," MRS Bulletin, **vol. 21**, no. 7, pp. 46–52, Jul. 1996, doi: 10.1557/S0883769400035910.

[3] F. J. Walker, R. A. McKee, H. Yen, and D. E. Zelmon, "Optical clarity and waveguide performance of thin film perovskites on MgO," Appl Phys Lett, **vol. 65**, no. 12, pp. 1495–1497, Sep. 1994, doi: 10.1063/1.112023.

[4] B. Bajac et al., "Structural characterization and dielectric properties of BaTiO3 thin films obtained by spin coating," Process Appl Ceram, **vol. 8**, no. 4, pp. 219–224, 2014, doi: 10.2298/PAC1404219B.

[5] A. Ianculescu, B. Despax, V. Bley, T. Lebey, R. Gavrilă, and N. Drăgan, "Structure–properties correlations for barium titanate thin films obtained by rf-sputtering," J Eur Ceram Soc, **vol. 27**, no. 2, pp. 1129–1135, Jan. 2007, doi: 10.1016/j.jeurceramsoc.2006.05.043.

[6] W. Preis and W. Sitte, "Modeling of electrical properties of grain boundaries in n-conducting barium titanate ceramics as a function of temperature and dc-bias," Solid State Ionics, vol. 262, pp. 486–489, Sep. 2014, doi: 10.1016/j.ssi.2013.10.062.

[7] N. Golego, S. A. Studenikin, and M. Cocivera, "Properties of Dielectric $BaTiO_3$ Thin Films Prepared by Spray Pyrolysis," Chem. Mater., **vol. 10**, no. 7, pp. 2000–2005, Jul. 1998, doi: 10.1021/cm980153+.

[8] Y. Liu, S. Li, F. Gallucci, and E. V. Rebrov, "Sol-gel synthesis of tetragonal BaTiO3 thin films under fast heating," Appl Surf Sci, **vol. 661**, p. 160086, Jul. 2024, doi: 10.1016/j.apsusc.2024.160086.

[9] K.-I. Park, S. Xu, G.-T. Hwang, S.-J.L. Kang, Z.L. Wang, and K.J. Lee, "Piezoelectric $BaTiO_3$ Thin Film Nanogenerator on Plastic Substrates," Nano Lett., **vol. 10**, no. 12, pp. 4939–4943, Dec. 2010, doi: 10.1021/nl102959k.

[10] S. Pal, S. Muthukrishnan, B. Sadhukhan, S. N. V., D. Murali, and P. Murugavel, "Bulk photovoltaic effect in $BaTiO_3$-based ferroelectric oxides: An experimental and theoretical study," J Appl Phys, **vol. 129**, no. 8, p. 084106, Feb. 2021, doi: 10.1063/5.0036488.

[11] W.-B. Li, D. Zhou, R. Xu, D.-W. Wang, J.-Z. Su, L.-X. pang, W.-F. Liu, and G.-H. Chen, "$BaTiO_3$-Based Multilayers with Outstanding Energy Storage Performance for High Temperature Capacitor Applications," ACS Appl. Energy Mater., **vol. 2**, no. 8, pp. 5499–5506, Aug. 2019, doi: 10.1021/acsaem.9b00664.

[12] S. Kappadan, T. W. Gebreab, S. Thomas, and N. Kalarikkal, "Tetragonal $BaTiO_3$ nanoparticles: An efficient photocatalyst for the degradation of organic pollutants," Mat Sci Semicon Proc, **vol. 51**, pp. 42–47, Aug. 2016, doi: 10.1016/j.mssp.2016.04.019.

[13] S. Yasmin, S. Choudhury, M. A. Hakim, A. H. Bhuiyan, and M. J. Rahman, "Structural and dielectric properties of pure and cerium-doped barium titanate," J. Ceram. Process. Res, **vol. 12**, no. 4, pp. 387–391, 2011.

[14] J. H. Hwang and Y. H. Han, "Electrical Properties of Cerium-Doped $BaTiO_3$," J Am Ceram Soc, **vol. 84**, no. 8, pp. 1750–1754, 2001, doi: 10.1111/j.1151-2916.2001.tb00910.x.

[15] M. Mostafa, M. J. Rahman, and S. Choudhury, "Enhanced dielectric properties of $BaTiO_3$ ceramics with cerium doping, manganese doping and Ce-Mn co-doping," Sci Eng Compos Mater, **vol. 26**, no. 1, pp. 62–69, Jan. 2019, doi: 10.1515/secm-2017-0177.

[16] N. Yasuda, H. Murayama, Y. Fukuyama, J. Kim, S. Kimura, K. Toriumi, Y. Tanaka, Y. Moritomo, Y. Kuroiwa, K. Kato, H. Tanaka, and M. Takata, "X-ray diffractometry for the structure determination of a submicrometre single powder grain," J Synchrotron Rad, **vol. 16**, no. 3, pp. 352–357, May 2009, doi: 10.1107/S090904950900675X.

[17] G. Canu, G. Confalonieri, M. Deluca, L. Curecheriu, M. T. Buscaglia, M. Asanduleasa, N. Horchidan, M. Dapiaggi, L. Mitoseriu, and V. Buscaglia, "Structure-property correlations and origin of relaxor behaviour in $BaCe_xTi_{1-x}O_3$," Acta Mater, **vol. 152**, pp. 258–268, Jun. 2018, doi: 10.1016/j.actamat.2018.04.038.

[18] A.-C. Ianculescu, D. C. Berger, C.A. Vasilescu, M. Olariu, B.S. Vasile, L.P. Curecheriu, A. Gajović, and R. Trușcă, "Incorporation Mechanism and Functional Properties of Ce-Doped BaTiO3 Ceramics Derived from Nanopowders Prepared by the Modified Pechini Method," in Nanoscale Ferroelectrics and Multiferroics, John Wiley & Sons, Ltd, 2016, pp. 13–43. doi: 10.1002/9781118935743.ch1.

[19] M. Cernea, I. Matei, A. Iuga, and C. Logofatu, "Preparation and characterization of Ce-doped $BaTiO_3$ thin films by r.f. sputtering," J Mater Sci, **vol. 36**, no. 20, pp. 5027–5030, Oct. 2001, doi: 10.1023/A:1011858319581.

[20] C. H. Jung, S. I. Woo, Y. S. Kim, and K. S. No, "Reproducible resistance switching for BaTiO3 thin films fabricated by RF-magnetron sputtering," Thin Solid Films, **vol. 519**, no. 10, pp. 3291–3294, Mar. 2011, doi: 10.1016/j.tsf.2010.12.149.

[21] M. Cernea, A. Ianculescu, O. Monnereau, L. Argéme, V. Bley, B. Bastide, and C. Logofatu, "Preparation and characterization of Ce-doped BaTiO3 thin films by pulsed laser deposition," J Mater Sci, **vol. 39**, no. 8, pp. 2755–2759, Apr. 2004, doi: 10.1023/B:JMSC.0000021450.39778.81.

[22] S. h. Mohamed and Z. H. and Dughaish, "Microstructural and optical investigations of Ce-doped barium titanate thin films by FTIR and spectroscopic ellipsometry," Philos Mag, **vol. 92**, no. 10, pp. 1212–1222, Apr. 2012, doi: 10.1080/14786435.2011.642320.

[23] J.-M. Oh and S.-M. Nam, "Thickness limit of $BaTiO_3$ thin film capacitors grown on SUS substrates using aerosol deposition method," Thin Solid Films, **vol. 518**, no. 22, pp. 6531–6536, Sep. 2010, doi: 10.1016/j.tsf.2010.03.159.

[24] O. Kreinin, N. P. Kuzmina, E. Zolotoyabko, and A. R. Kaul, "Rapid thermal two-stage metal-organic chemical vapor deposition growth of epitaxial $BaTiO_3$ thin films," Thin Solid Films, **vol. 515**, no. 16, pp. 6442–6446, Jun. 2007, doi: 10.1016/j.tsf.2006.11.051.

[25] S.-S. Park, J.-H. Ha, and H. N. Wadley, "Preparation of $BaTiO_3$ films for MLCCs by direct vapor deposition," Integr Ferroelectr, Dec. 2007, doi: 10.1080/10584580701759437.

[26] M. Cernea, O. Monnereau, P. Llewellyn, L. Tortet, and C. Galassi, "Sol–gel synthesis and characterization of Ce doped-BaTiO3," J Eur Ceram Soc, **vol. 26**, no. 15, pp. 3241–3246, Jan. 2006, doi: 10.1016/j.jeurceramsoc.2005.09.039.

[27] Y. Iriani, A. Suparmi, A. Marzuki, and D.K. Sandi, "Microstructures and Optical Properties of Nanocrystalline Pr- doped $BaTiO_3$ Thin Film," Int. J. Thin.Film. Sci. Tec., **vol. 11**, no. 3, pp. 307–311, Sep. 2022, doi: 10.18576/ijtfst/110307.

[28] C. Ang, Z. Jing, and Z. Yu, "Ferroelectric relaxor $Ba(Ti,Ce)O_3$," J. Phys.: Condens. Matter, **vol. 14**, no. 38, p. 8901, Sep. 2002, doi: 10.1088/0953-8984/14/38/313.

[29] D. A. G. Bruggeman, "Berechnung verschiedener physikalischer Konstanten von heterogenen Substanzen. I. Dielektrizitätskonstanten und Leitfähigkeiten der Mischkörper

aus isotropen Substanzen," Annalen der Physik, **vol. 416**, no. 7, pp. 636–664, 1935, doi: 10.1002/andp.19354160705.

[30] L. V. Maneeshya, S. S. Lekshmy, P. V. Thomas, and K. Joy, "Europium incorporated barium titanate thin films for optical applications," J Mater Sci: Mater Electron, **vol. 25**, no. 6, pp. 2507–2515, Jun. 2014, doi: 10.1007/s10854-014-1903-5.

[31] A. Karvounis, F. Timpu, V. V. Vogler-Neuling, R. Savo, and R. Grange, "Barium Titanate Nanostructures and Thin Films for Photonics," Adv Opt Mater, **vol. 8**, no. 24, p. 2001249, Dec. 2020, doi: 10.1002/adom.202001249.

[32] S. Goswami and A. K. Sharma, "Investigation of the optical behavior of indium oxide thin films with the aid of spectroscopic ellipsometry technique", Appl. Surf. Sci., **vol. 495**, p. 143609, Nov. 2019, doi: 10.1016/j.apsusc.2019.143609.

[33] D. M. Dieter Mergel and A. M. J. Martin Jerman, "Density and refractive index of thin evaporated films," Chin. Opt. Lett., **vol. 8,** no. S1, pp. 67–72, 2010, doi: 10.3788/COL201008S1.0067.

[34] D. Mergel, "Modeling thin TiO_2 films of various densities as an effective optical medium," Thin Solid Films, **vol. 397**, no. 1, pp. 216–222, Oct. 2001, doi: 10.1016/S0040-6090(01)01403-1.